Electronic band structure of Mg-IV-N_2 compounds in the quasiparticle-self-consistent GW approximation

Atchara Punya Jaroenjittichai
Department of Physics and Materials Science, Faculty of Science, Chiang Mai University, 239 Huay Kaew Road, Muang, Chiang Mai 50200, Thailand

Walter R. L. Lambrecht
Department of Physics, Case Western Reserve University, 10900 Euclid Avenue, Cleveland, Ohio 44106-7079, USA
(Received 25 June 2016; published 9 September 2016; corrected 28 September 2016)

We present calculations of the lattice constants, structural parameters, bulk moduli, energies of formation, and band structures of Mg-IV-N_2 compounds with IV=Si, Ge, Sn by using the full-potential linearized muffin-tin orbital method and the quasiparticle-self-consistent GW approach for the wurtzite-based $Pna2_1$ crystal structure. The lattice parameters calculated with the generalized gradient approximation (GGA) are found to be in good agreement (within 1%) with experiment for the cases of $MgSiN_2$ and $MgGeN_2$, where data are available. Similar to the Zn-IV-N_2 compounds, $MgSiN_2$ is found to have an indirect gap slightly lower than the lowest direct gap, while the other materials have direct gaps. The direct gaps, calculated at the GGA lattice constant, range from 3.43 eV for $MgSnN_2$ to 5.14 eV for $MgGeN_2$ and 6.28 eV for $MgSiN_2$ in the 0.8Σ approximation, i.e., reducing the QSGW Σ by a factor 0.8 and including an estimated zero-point-motion correction. The symmetry character of the valence-band maximum states and their splittings and effective masses are determined. The conduction-band minima are found to have slightly higher Mg s- than Si s-like character in $MgSiN_2$ but in $MgGeN_2$ and $MgSnN_2$, the group-IV-s character becomes increasingly dominant.

DOI: 10.1103/PhysRevB.94.125201

I. INTRODUCTION

The heterovalent ternary nitride materials of formula II-IV-N_2 are of considerable interest to complement the family of binary group-III nitrides. They are formally derived from them by replacing the group-III element by alternating group-II and group-IV elements in such a way as to locally preserve neutrality or the octet bonding rule. Because the group-III nitrides occur naturally in the wurtzite structure, the so-derived compounds are expected to form in a wurtzite-derived ordered superstructure. Several of these compounds have indeed been found to occur in the so-called β-$NaFeO_2$ structure, which has the space group $Pna2_1$. Although disordered wurtzite structures, and a smaller-unit-cell crystal structure with space group $Pmc2_1$ structure, have also been considered [1], the latter has not yet been observed experimentally. This 16-atom $Pna2_1$ structure is the analog for wurtzite of the ternary chalcopyrite structure for the zinc blende binary. The chalcopyrite structure is commonly found for other II-IV-V_2 compounds with V other than N. An overview of the history of these ternary nitride compounds can be found in Ref. [2].

While some of these materials were already synthesized in the 1960–1970s, for most of them only the crystal structure was determined at that time and their physical properties are still largely unknown. In recent years, the Zn-based compounds, $ZnSiN_2$, $ZnGeN_2$, and $ZnSnN_2$ have started to be explored as semiconductor materials [3–6]. $ZnSnN_2$ was only synthesized in the last few years and was pursued as a suitable material for photovoltaic applications because it consists only of sustainable and abundantly available elements and its gap which was initially estimated to be of order 1.4 eV [7–9]. Subsequent work showed that its gap is actually larger [9]: 1.7 eV, but possibly disorder can reduce the gap and still make it suitable for the intended solar-cell applications [10]. The band gap of $ZnGeN_2$ is close to that of GaN and as such suitable for opto-electronic and other wide-band-gap-semiconductor applications. GaN and related nitrides have notably found use in light-emitting diodes (LED) and blue lasers. The importance of the development of white LEDs for energy conservation was recognized with the Nobel prize in physics in 2014. The good lattice match between $ZnGeN_2$ and GaN and similar gaps but with a sizable band offset [11] was shown to be potentially useful in LED design [12]. The defect physics in these materials is also significantly different from III nitrides and hence lends itself possibly to new opportunities for doping [13]. Thus, the group-II-IV-N_2 nitrides add considerable new flexibility to band-gap engineering and defect engineering. From a fundamental-science point of view, the larger unit cell and lower symmetry leads to a much more complex phonon spectrum [14–17] and additional anisotropies of the near band gap optical properties. The spontaneous polarizations and piezo-electric properties of the Zn-IV-N_2 compounds were studied in Ref. [18]. The band structure of the Zn-IV-N_2 compounds was calculated by using the quasiparticle-self-consistent (QS) GW method by Punya *et al.* [19].

As these materials contain two cations of different valence, there is more room to explore in chemical parameter space. It is thus of interest to study other group-II-IV-N_2 semiconductors. For example, it was already predicted that $CdGeN_2$ would have a band gap corresponding to the green portion of the visible spectrum [20]. On the other hand, replacing Zn by Mg may be expected to lead to larger band gaps in the UV region and could thus possibly be useful to extend the opto-electronic properties of nitrides into the deeper UV region. While AlN already has a gap of 6.2 eV, it has been found difficult to dope such a wide-gap material and pushing $Al_xGa_{1-x}N$ alloys to deeper UV is hindered by the lattice mismatch for higher Al concentrations.

This forms the motivation of the present study of Mg-IV-N_2 compounds. Among these materials, $MgSiN_2$ and $MgGeN_2$ have already been grown [21] but, as noted before, not much is known about their physical properties besides their crystal structure. $MgSnN_2$ has to the best of our knowledge not been synthesized yet. Since the pioneering work of David *et al.* [21], $MgSiN_2$ ceramic samples were synthesized by Bruls *et al.* [22–24] and studied mainly in terms of their thermal properties as possible substrates for integrated circuits as a replacement for AlN. Work on ceramic samples of $MgSiN_2$ was also reported by Lenčěš *et al.* [25]. Several previous computational studies were performed [26–31] but most of these studies used density functional theory in the local density approximation, which is not reliable for band gaps. The purpose of this study is to start filling this lack of knowledge by calculating their electronic band structure with a reliable predictive approach. To this end we use the so-called quasiparticle-self-consistent GW method [32].

II. METHODS

Density functional theory in the local density approximation (LDA) as well as the generalized gradient approximation (GGA) are used to optimize the lattice constants and atomic positions inside the unit cell. These calculations are carried out by using the ABINIT code [33]. A plane-wave cutoff energy of 80 Hartree and a $4 \times 4 \times 4$ $\boldsymbol{k}$-point mesh was used. LDA and GGA pseudopotential are generated from the fhi98PP code [LDA Ceperley–Alder-Perdew-Wang (1992) [34] and GGA-PBE Perdew–Burke–Ernzerhof (1996) [35]]. The pseudopotentials used were of the Trouiller–Martins type and generated by Fuchs and Scheffler [36].

In the self-consistent PBE-GGA band-structure calculations, we used a full-potential linearized muffin-tin orbital (FP-LMTO) method [37,38]. The Brillouin-zone integration was sampled on a $4 \times 4 \times 4$ $\boldsymbol{k}$-point mesh. The basis set contains two sets of smoothed Hankel functions, decay parameters κ, and smoothing radii R_{sm}. For Mg, the basis set used consists of s and p functions for the first κ, R_{sm} and only s for the second set. In addition, the Mg-2p states were treated as local orbitals. For Si, Ge, Sn, and N we used an spd-sp set. Adding Mg-d basis functions had negligible effect on the band gaps and total energies. The augmentation of the basis functions inside the muffin-tin spheres, i.e., matching combinations of radial functions ϕ_{Rl} and its energy derivative $\dot{\phi}_{Rl}$ at the linearization energy to the basis envelope function, is carried out to $l_{\max} = 4$.

The quasiparticle band structure is calculated by using the quasiparticle self-consistent GW (or QSGW) approach implemented in the same FP-LMTO method as described in Refs. [32,39,40]. In this method, the self-energy $\Sigma(\boldsymbol{k},\omega)$ calculated from the Green's function G_0 and screened Coulomb interaction W_0 corresponding to a starting Hamiltonian H_0 is used to extract a Hermitian quasiparticle-exchange-correlation potential,

$$V_{ij}^{xc\text{-}QSGW} = \tfrac{1}{2}\mathrm{Re}[\Sigma_{ij}(\epsilon_i) + \Sigma_{ij}(\epsilon_j)], \quad (1)$$

in the basis of the eigenstates of H_0, which is then added back to H_0 and iterated until convergence. The result is thus independent of the starting H_0 (for which we choose either LDA or GGA-PBE). A $3 \times 3 \times 3$ $\boldsymbol{k}$ mesh was used for calculating the self-energy, $\Sigma_{ij}(\boldsymbol{k},\omega)$. The maximum energy used for calculating $\Sigma_{ij}(E_{cut}) = 2.5$ Ryd, above which it is approximated by a diagonal approximation and to depend linearly vs the H_0 eigenvalues. The reason for this is explained in Ref. [40]. $V_{ij}^{xc\text{-}QSGW}(\boldsymbol{k})$ can then be expanded in the muffin-tin orbital basis set and Fourier transformed to real space and then inverse Fourier transformed back to any $\boldsymbol{k}$ point, either to a finer mesh or to points along symmetry lines. This allows for an accurate interpolation of the full QSGW bands and also to obtain accurate effective masses.

III. RESULTS

A. Lattice constants, energies of formation, and bulk moduli

The lattice constants obtained by using LDA and GGA-ABINIT are given in Table I. For $MgSiN_2$, the GGA (PBE) and LDA (CAPZ) lattice constants [31] calculated with a plane-wave basis set as implemented in the CASTEP program are given in parentheses. We can see that LDA underestimates the volume, while GGA slightly overestimates it, as usual. The deviation of the lattice constants from the experiment by considering the volume errors shows that GGA results are closer to the experiments than those of LDA and those from Ref. [31]. The ratios b/a and c/a seem to be slightly

TABLE I. Lattice parameters a, b, and c (Å), lattice volume V (Å^3), the average error with respect to experiment ($\sigma = [(V/V_{\text{expt}}) - 1]/3$), and lattice constant ratio ($a_w = a/2$) in Mg-IV-N_2.

Compound		LDA-ABINIT	GGA-ABINIT	Expt.
$MgSiN_2$	a	6.374 (6.416)[a]	6.468(6.508)	6.473[b]
	b	5.209(5.219)	5.297(5.291)	5.272
	c	4.923(4.945)	5.012(5.015)	4.986
	V	163.47(165.58)	171.70(172.68)	170.15
	$\frac{V}{V_{\text{expt}}}$	0.96	1.01	
	σ	−0.013	0.003	
	b/a_w	1.635	1.638	1.628
	c/a_w	1.545	1.550	1.541
$MgGeN_2$	a	6.499	6.639	6.610[c]
	b	5.389	5.540	5.490
	c	5.070	5.212	5.170
	V	177.55	191.72	187.61
	$\frac{V}{V_{\text{expt}}}$	0.95	1.02	
	σ	−0.018	0.007	
	b/a_w	1.658	1.669	1.661
	c/a_w	1.560	1.570	1.564
$MgSnN_2$	a	6.712	6.905	
	b	5.746	5.932	
	c	5.313	5.499	
	V	204.90	225.23	
	b/a_w	1.712	1.718	
	c/a_w	1.583	1.593	

[a]In parentheses obtained from Ref. [31].
[b]$MgSiN_2$ data taken from Ref. [24].
[c]$MgGeN_2$ data taken from Inorganic Crystal Structure Database (ICSD) [41].

TABLE II. Wyckoff 4(a) positions (reduced coordinates) in the unit cell.

Compound	Atoms	x	y	z
$MgSiN_2$	Mg	0.623 (0.623,[a] 0.623[b])	0.085 (0.084, 0.085)	0.000 (0.000, 0.000)
	Si	0.125 (0.125, 0.125)	0.070 (0.070, 0.069)	0.011 (0.012, 0.014)
	N_{Si}	0.096 (0.094, 0.096)	0.049 (0.047, 0.049)	0.359 (0.358, 0.362)
	N_{Mg}	0.655(0.657, 0.655)	0.109 (0.110, 0.109)	0.421 (0.424, 0.425)
$MgGeN_2$	Mg	0.623	0.085	0.000
	Ge	0.126	0.074	0.007
	N_{Ge}	0.108	0.061	0.368
	N_{Mg}	0.642	0.100	0.404
$MgSnN_2$	Mg	0.624	0.083	0.000
	Sn	0.126	0.083	0.003
	N_{Sn}	0.122	0.079	0.382
	N_{Mg}	0.627	0.085	0.384

[a]Calculation from Ref. [31].
[b]Experiment from Ref. [24].

overestimated in GGA and closer in LDA, but even in GGA they differ by less than 1%. Thus the band structures and related properties will be calculated by using the GGA (PBE) lattice constants. For $MgSnN_2$, to the best of our knowledge, no experimental data are available.

Based on x-ray diffraction, $MgSiN_2$ has space group $Pna2_1$. Each of the atoms, Mg, Si, N_1 (above Mg) and N_2 (above Si) occur in Wyckoff (4a) positions, with reduced coordinates, (x,y,z), $(-x,-y,z+1/2)$, $(x+1/2,-y+1/2,z)$, and $(-x+1/2,y+1/2,z+1/2)$, where the origin is chosen to lie on the two-fold screw axes parallel to the c axis. The z location of the origin is arbitrary and we choose it to make the z positions of Mg be zero. The parameters describing each type of atom's reduced coordinates (x,y,z) and obtained by minimizing the total energy as a function of these parameters by a molecular statics relaxation using a conjugate gradient method are given in Table II. This relaxation was carried out within the GGA (PBE) approach by using the FP-LMTO method after a full relaxation of lattice constants and internal coordinates using the ABINIT method. The two methods agree closely on the Wyckoff positions once the lattice constants are fixed. Our calculated atomic positions of $MgSiN_2$ obtained from GGA (PBE) are compared with those from Ref. [31] and with experimental values from Ref. [24] in parentheses in Table II. For the other compounds, no other data are available to compare with.

The average bond lengths and the formation energies are reported in Table III and are in good agreement with Arab *et al.* [31] and with experimental data for $MgSiN_2$. We also obtained the equilibrium bulk moduli and their first pressure derivatives by fitting the total energy versus volume per formula unit to the Vinet equation of state [42]. The formation energies per formula unit calculated here are defined with respect to Mg in hexagonal close packed structure, Si, Ge, and Sn in diamond structure, and N_2 as a gas molecule. The cohesive energies per atom based on GGA calculations corresponding to Mg, Si, Ge, Sn, and the binding energy of a N_2 molecule are -1.42, -5.40, -4.49, -3.74, and -8.45 eV, respectively.

B. Band structures

The band structures of Mg-IV-N_2 calculated within the QSGW method and at the GGA (PBE) lattice constants are shown in Fig. 1. Their corresponding total- and partial-wave resolved densities (PDOS) of states are shown in Fig. 2. The PDOS are summed over all equivalent atoms in the cell, so over all four Mg, all four IV, and all eight N atoms. The reason why they do not add up to the total is that the total also includes the interstitial contribution. As expected, they show the upper valence band has mainly N-2p-bonding character with Mg and group-IV s and p states. The group-IV s states have their largest contribution to the bonding states in the lower-energy region of the upper valence band, around -8 eV. The density of states at the bottom of the conduction band is low because of the large dispersion of the lowest conduction band (small electron effective mass). It has mostly Mg-s character in the $MgSiN_2$ case, but also a higher Ge-s and Sn-s character in the corresponding compounds. In fact, inspecting the actual contribution of the IV-s vs Mg-s basis function to the eigenstate of the conduction-band minimum (CBM) at Γ shows that the ratio of the IV-s contribution to the Mg-s contribution is 0.83 in the case of $MgSiN_2$, 1.48 in the case of $MgGeN_2$, and 2.80 in the case of $MgSnN_2$. This is illustrated for the case of $MgGeN_2$

TABLE III. Average bond lengths in Å, formation energies (E_f) in eV per formula unit, bulk moduli in GPa and their pressure derivatives obtained from fitting the Vinet equation of state.

Compound	Mg-N (Å)	IV-N (Å)	E_f (eV)	B (GPa)	B′
$MgSiN_2$	2.10	1.76	-7.60	194	4.3
	(2.11 [31], 2.09 [23])	(1.75 [31],1.75 [23])	(-6.38 [31])	(171 [31])	(3.82 [31])
$MgGeN_2$	2.09	1.88	-4.14	158	4.8
$MgSnN_2$	2.10	2.08	-3.41	134	4.9

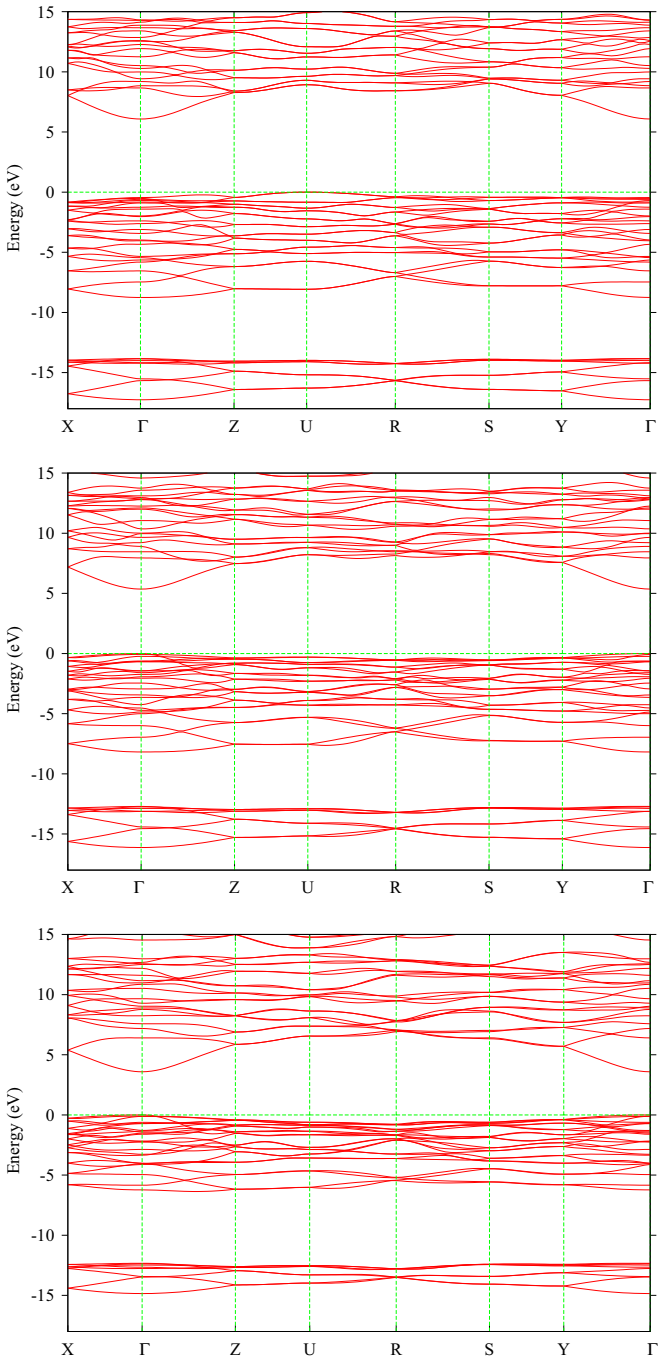

FIG. 1. QSGW electronic band structure of $MgSiN_2$, $MgGeN_2$ and $MgSnN_2$.

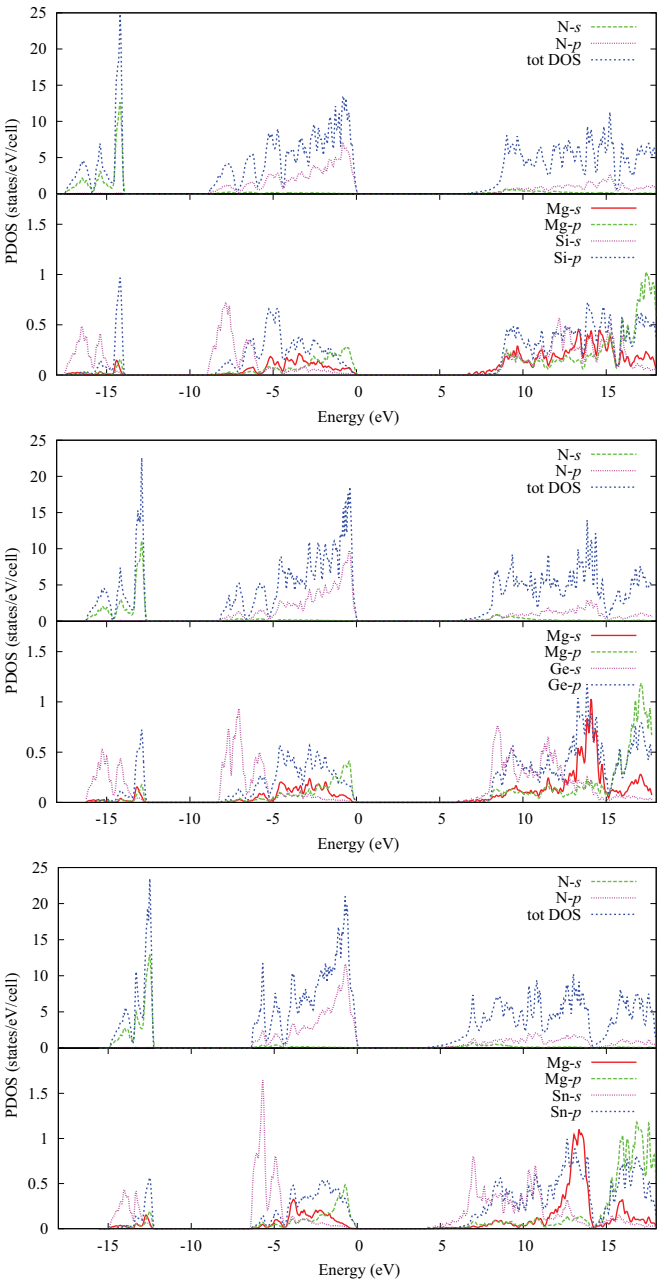

FIG. 2. Total and partial densities of states : N-2s, -2p, IV -ns, -np, with $n = 3,4,5$ for Si, Ge, Sn, Mg-3s, -3p, of $MgSiN_2$, $MgGeN_2$, and $MgSnN_2$.

in Fig. 3. Please note the different color scales in both figures, which are normalized according to the maximum contribution for the Mg-s contribution. Thus the CBM becomes increasingly more IV-s like as we go from Si to Ge to Sn, starting out with a a state which is slightly more Mg-s like.

The band gaps are given in Table IV in various approximations. As mentioned earlier, our band gaps of Mg-IV-N_2 are all calculated at the GGA lattice constants. The Kohn–Sham DFT-GGA band gaps of $MgSiN_2$ and $MgGeN_2$ are comparable to those calculated by LDA and by using the PWscf program by Basalaev *et al.* [28]. The QSGW gaps are significantly larger. Because the QSGW method tends to overestimate the gaps systematically by its underestimate of the dielectric screening, we report the so-called 0.8Σ result, where the $\Delta V^{xc\text{-}QSGW} = V^{xc\text{-}QSGW} - V^{xc\text{-}GGA}$ is multiplied by a factor 0.8. This *ad hoc* reduction factor has been found to work well to correct the gaps for most tetrahedrally bonded semiconductors. The calculated band gaps of $MgSiN_2$ in the 0.8Σ approach are close to those of the hybrid Heyd-Scuseria-Ernzerhof (HSE) [43,44] functional by Quirk *et al.* [45], which are 5.7 eV (indirect) and 6.3 eV (direct).

We estimate the zero-point motion corrections [$\Delta(0)$] by using reported values by Cardona and Thewalt [46] for the

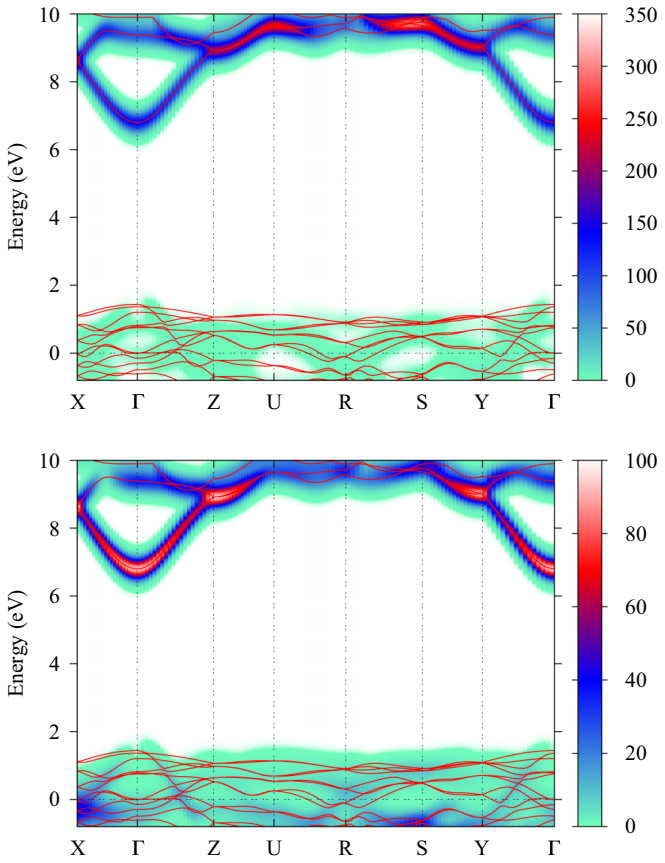

FIG. 3. Bands of $MgGeN_2$ near the gap colored according to their Ge-*s* (top) and Mg-*s* (bottom) LMTO-basis-function content. The color scale is normalized to 100% according to the maximum for the Mg-*s* content in both cases.

III-N semiconductors. As pointed out in Punya *et al.* [19] $\Delta(0)$ is approximately proportional to the band gap itself given by $\Delta(0) = -50 - 31E_g$ meV in the family of the III-N compounds. Thus, $\Delta(0)$ for $MgSiN_2$, $MgGeN_2$, and $MgSnN_2$ are estimated to be -238 (-252), -216, and -161 meV, respectively. We omit the exciton binding energy since it is only of order 10–20 meV in the related Zn-IV-N_2 compounds, which is below the remaining uncertainty at this point coming from the 0.8Σ approximation.

Since our band gaps are calculated at the GGA lattice constants which slightly overestimate the experimental values, one expects the gaps to be slightly underestimated. To estimate this effect, we calculate the band-gap deformation potentials (in the GGA). The band-gap deformation potential is the change in gap per percentage change in volume. The deformation potentials for $MgSiN_2$, $MgGeN_2$, and $MgSnN_2$ are -8.7, -7.7, and -4.4 eV, respectively. The minus sign shows that the band gap decreases when the lattice constant increases. So, for $MgSiN_2$, our lattice volume is overestimated by 0.009 and the gap could thus be underestimated by $0.009 \times 8.7 \approx 0.08$ eV. For $MgGeN_2$ our lattice volume is overestimated by by 0.021, so the gap could be underestimated by 0.16 eV. Thus, the uncertainty due to the lattice constants results in an uncertainty in the gaps of at most 0.2 eV. The band-gap deformation potentials are included in Table IV. At present no experimental values are available to compare with.

As expected, the band gaps of the Mg-IV-N_2 compounds are significantly larger than those of the corresponding Zn compounds. Interestingly, the $MgSnN_2$ compound has a gap close to that of $ZnGeN_2$ or GaN. This could be of interest from a sustainability point of view because $MgSnN_2$ is constituted completely from widely abundant elements. The other compounds have gaps which extend their usefulness significantly in to the deeper UV. The direct gaps of $ZnGeN_2$ and $ZnSiN_2$ correspond to 241 and 197 nm, respectively. The lowest direct gap of $MgSiN_2$ is found to be very close to that of wurtzite AlN, but it has a 0.44 eV lower indirect gap. This is due to the shift of the valence-band maximum (VBM) to a different $\boldsymbol{k}$ point, namely at the point U in the Brillouin zone. A similar shift of the VBM away from Γ was found in $ZnSiN_2$, although in that case, the VBM occurs near Y [19].

C. Valence-band splittings and effective masses

Next, we inspect the band structure in more detail near the valence-band maximum in Fig. 4. The states at Γ are labeled according to the irreducible representations of the C_{2v} group. Here, a_1 corresponds to z, b_1 to x, and b_2 to y. a_2 corresponds to xy. We can see that, for the $MgGeN_2$ and $MgSnN_2$ cases, the highest VBM has a_1 symmetry. This is similar to AlN, where the highest valence-band maximum has the Γ_1 symmetry of wurtzite, which also corresponds to the z axis perpendicular to the basal plane or along the c axis of the wurtzite structure. It is related to c/a value, which is lower than the ideal value of $\sqrt{8/3}$. This determines the sign of the crystal-field splitting to be negative. It is usually defined as $\Delta_c = \Gamma_5 - \Gamma_1$ in wurtzite structures. In the orthorhombic structure of the present materials, the wurtzite Γ_5 further splits in a b_1 and b_2 state. We can see that, in both cases, $b_2 > b_1$ but the splitting is small in the Sn compound and large in the Ge compound so that the b_2 state ends up closer to the a_1 state than to the b_1 state below it. In $MgSiN_2$, the situation is more complex because the actual VBM occurs at U. This is different

TABLE IV. Band gaps of Mg-IV-N_2 compounds in various approximations and band-gap deformation potentials.

Compound		LDA[a]	HSE[b]	GGA	0.8Σ	$0.8\Sigma + \Delta(0)$[c]	$dE_g/d\ln V$
$MgSiN_2$	Indirect	4.32	5.7	4.01	6.08	5.84	−8.7
	Direct	4.56	6.3	4.44	6.53	6.28	
$MgGeN_2$	Direct	3.01		2.67	5.36	5.14	−7.7
$MgSnN_2$	Direct			1.16	3.59	3.43	−4.4

[a]From Ref. [28].
[b]From Ref. [45].
[c]$\Delta(0)$ is the estimated zero-point motion renormalization correction (see text).

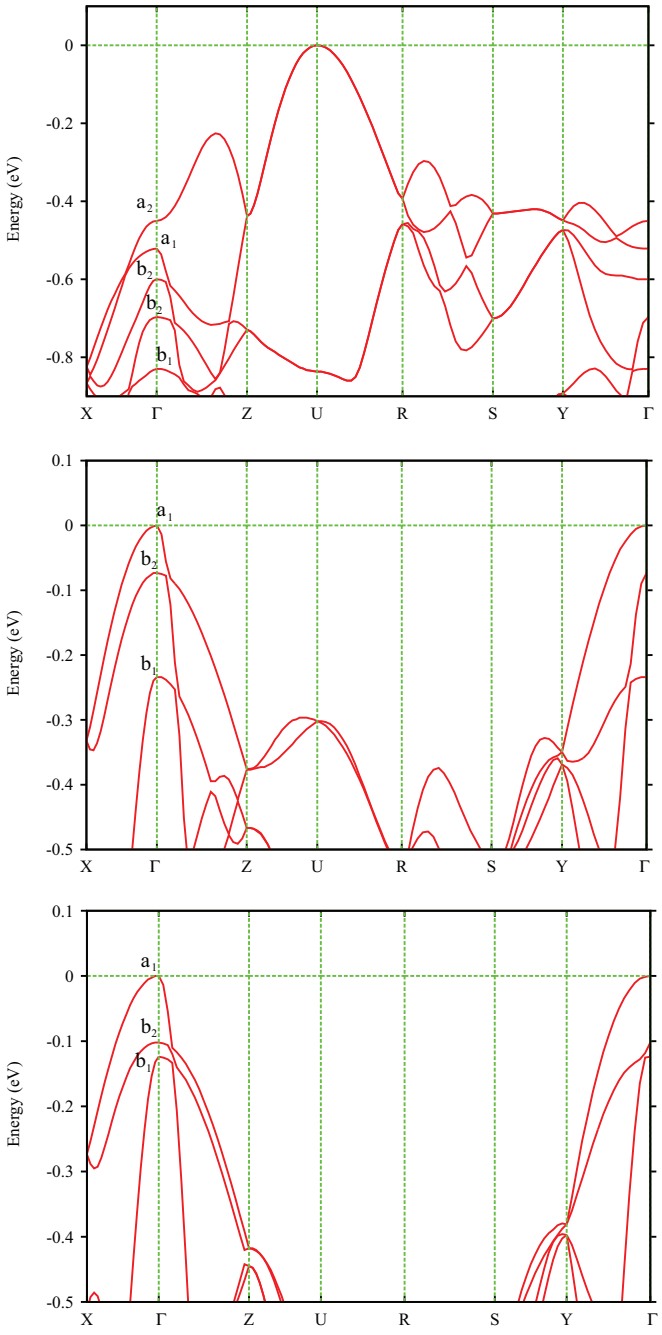

FIG. 4. Fine structure of the bands near the valence band maximum with symmetry labeling at Γ for $MgSiN_2$, $MgGeN_2$, and $MgSnN_2$.

from $ZnSiN_2$ where an indirect gap also occurs but with a VBM near Y. Apparently, the lower Si states hybridize stronger with the N-2p bands and several states of other symmetry occur at Γ with the actual VBM at Γ having a_2 symmetry. The splittings are summarized in Table V.

In the $MgGeN_2$ and $MgSnN_2$ case, the VBM splittings and effective masses can be described in terms of an extension of the Kohn–Luttinger effective Hamiltonian, generalized in our previous paper [19] for the orthorhombic symmetry. In Table VI we give the effective masses in the x, y, z directions for each split VB state, as well as those of the CBM. Finally, in Table VII we give the KL-parameters for these two materials

TABLE V. Valence-band splittings (in meV) at the Γ point relative to actual VBM.

Symmetry	$MgSiN_2$	$MgGeN_2$	$MgSnN_2$
a_2	−450.0		
a_1	−521.1	0	0
b_2	−600.0	− 73.5	− 102.0
b_2	−696.6		
b_1	−829.8	− 234.0	− 123.8

TABLE VI. Electron effective masses (in units of free electron mass m_e); note that in the VBM they are negative, indicating positive hole masses. For $MgSiN_2$, we indicate the VBM masses at the U VBM, for the other ones we indicate the masses of identified state near the VBM.

		$MgSiN_2$	$MgGeN_2$	$MgSnN_2$
CBM at Γ	m_x^c	0.32	0.31	0.26
	m_y^c	0.33	0.30	0.26
	m_z^c	0.34	0.28	0.24
VBM at Γ	$m_x^{a_1}$		− 2.34	− 2.85
	$m_y^{a_1}$		− 3.34	− 3.18
	$m_z^{a_1}$		− 0.25	− 0.23
	$m_x^{b_1}$		− 0.34	− 0.27
	$m_y^{b_1}$		− 5.40	− 4.78
	$m_z^{b_1}$		− 2.83	− 3.14
	$m_x^{b_2}$		− 2.20	− 3.71
	$m_y^{b_2}$		− 0.29	− 0.26
	$m_z^{b_2}$		− 3.40	− 3.33
VBM at U	m_x^v	− 1.68		
in $MgSiN_2$	m_y^v	− 2.27		
	m_z^v	− 0.82		

TABLE VII. Parameters of effective Hamiltonian: inverse-mass parameters A_i, B_i, C_i ($\hbar^2/2m_e$), energy splitting (meV).

Parameter	$MgGeN_2$	$MgSnN_2$
A_1	− 4.01	− 4.41
A_2	3.69	4.10
A_3	0.03	0.01
B_1	− 0.36	− 0.33
B_2	− 1.40	− 1.67
B_3	− 0.18	− 0.05
C_1	− 0.06	− 0.02
C_2	0.11	0.04
C_3	1.44	1.76
D_1	2.88	3.53
D_2, D_3	2.08	2.95
Δ_{1c}	− 153.7	− 112.9
Δ_{2c}	− 80.3	− 10.9

by using the parameters described in Ref. [19]. For $MgSiN_2$, we provide instead the valence-band masses at the actual VBM at U. The Kohn–Luttinger Hamiltonian in that case does not make sense because, instead, a more complex five-band Hamiltonian (or 10-band Hamiltonian including spin) would be needed to describe the valence-band manifold at Γ. In fact, this Hamiltonian is less relevant because the actual VBM occurs 450 meV above the one at Γ. This is much larger than room temperature so holes will likely stay confined to the neighborhood of the U point. This band is doubly degenerate and slightly anisotropic.

IV. CONCLUSIONS

In summary, in this paper, we have calculated the lattice constants and structural parameters of the Mg-IV-N_2 family of compounds. They were found to be in good agreement with experiments and previous calculations for the $MgSiN_2$ and $MgGeN_2$ cases and provide a prediction for the $MgSnN_2$ compound, which remains to be synthesized. We have calculated their band structures in the QSGW approximation which provides accurate predictions for the band gaps of these compounds. They are found to be potentially useful for UV opto-electronics. The $MgGeN_2$ and $MgSnN_2$ compounds are found to have direct gaps in the UV region, with that of $MgSnN_2$ close to that of GaN (3.4 eV) and that of $MgGeN_2$ (5.14 eV) somewhat lower than that of AlN. $MgSiN_2$ is found to have a direct gap close to that of AlN (6.3 eV), but has a substantially lower indirect gap at 5.84 eV. Details of the valence-band splittings due to the lower symmetry and effective masses were determined.

Note added in proof. The recent Heyd-Scuseria-Ernzerhof hybrid functional calculation by Quirk *et al.* [45] provides band gaps for $MgSiN_2$ in excellent agreement with our calculation.

ACKNOWLEDGMENTS

The work of A.P.J. was supported by Thailand Research Fund under Grant No. 5880193; the work of W.R.L. was supported by the U.S. National Science Foundation under Grant No. DMR-1533957. Calculations made use of the High Performance Computing Resource in the Core Facility for Advanced Research Computing at Case Western Reserve University.

[1] P. C. Quayle, E. W. Blanton, A. Punya, G. T. Junno, K. He, L. Han, H. Zhao, J. Shan, W. R. L. Lambrecht, and K. Kash, Phys. Rev. B **91**, 205207 (2015).

[2] W. R. L. Lambrecht and A. Punya, in *III-Nitride Semiconductors and their Modern Devices*, edited by B. Gill (Oxford University Press, Oxford, 2013), Chap. 15, pp. 519–585.

[3] L. Zhu, P. Maruska, P. Norris, P. Yip, and L. Bouthillette, MRS Internet J. Nitride Semicond. Res. **4S1**, G3.8 (1999).

[4] K. Du, C. Bekele, C. C. Hayman, J. C. Angus, P. Pirouz, and K. Kash, J. Cryst. Growth **310**, 1057 (2008).

[5] S. J. Pearton, M. E. Overberg, C. R. Abernathy, N. A. Theodoropoulou, A. F. Hebard, S. N. G. Chu, A. Osinsky, V. Fuflyigin, L. D. Zhu, A. Y. Polyakov, and R. G. Wilson, J. Appl. Phys. **92**, 2047 (2002).

[6] A. Osinsky, V. Fufluigin, L. D. Zhu, L. D. Goulakov, J. Graff, and E. Schubert, in *2000 IEEE/Cornell Conference on High Performance Devices* (IEEE, Piscataway, NJ, 2000), pp. 168–172.

[7] L. Lahourcade, N. C. Coronel, K. T. Delaney, S. K. Shukla, N. A. Spaldin, and H. A. Atwater, Adv. Mater. **25**, 2562 (2013).

[8] N. Feldberg, B. Keen, J. D. Aldous, D. Scanlon, P. A. Stampe, R. Kennedy, R. Reeves, T. D. Veal, and S. Durbin, in *38th IEEE Photovoltaic Specialists Conference (PVSC), 2012* (IEEE, Piscataway, NJ, 2012), pp. 002524–002527.

[9] P. C. Quayle, K. He, J. Shan, and K. Kash, MRS Commun. **3**, 135 (2013).

[10] N. Feldberg, J. D. Aldous, W. M. Linhart, L. J. Phillips, K. Durose, P. A. Stampe, R. J. Kennedy, D. O. Scanlon, G. Vardar, R. L. Field, T. Y. Jen, R. S. Goldman, T. D. Veal, and S. M. Durbin, Appl. Phys. Lett. **103**, 042109 (2013).

[11] A. Punya and W. R. L. Lambrecht, Phys. Rev. B **88**, 075302 (2013).

[12] L. Han, K. Kash, and H. Zhao, Proc. SPIE **9003**, 90030W (2014).

[13] D. Skachkov, A. Punya Jaroenjittichai, L.-y. Huang, and W. R. L. Lambrecht, Phys. Rev. B **93**, 155202 (2016).

[14] T. R. Paudel and W. R. L. Lambrecht, Phys. Rev. B **76**, 115205 (2007).

[15] T. R. Paudel and W. R. L. Lambrecht, Phys. Rev. B **78**, 115204 (2008).

[16] T. J. Peshek, T. R. Paudel, K. Kash, and W. R. L. Lambrecht, Phys. Rev. B **77**, 235213 (2008).

[17] W. R. L. Lambrecht, E. Alldredge, and K. Kim, Phys. Rev. B **72**, 155202 (2005).

[18] T. R. Paudel and W. R. L. Lambrecht, Phys. Rev. B **79**, 245205 (2009).

[19] A. Punya, W. R. L. Lambrecht, and M. van Schilfgaarde, Phys. Rev. B **84**, 165204 (2011).

[20] A. Punya and W. R. L. Lambrecht, Mater. Sci. Forum **717–720**, 1331 (2012).

[21] J. David, Y. Laurent, and J. Lang, Bull. Soc. Fr. Mineral. Cristallogr. **93**, 153 (1970).

[22] R. J. Bruls, H. T. Hintzen, and R. Metselaar, J. Mater. Sci. **34**, 4519 (1999).

[23] R. Bruls, H. Hintzen, R. Metselaar, and C.-K. Loong, J. Phys. Chem. Solids **61**, 1285 (2000).

[24] R. Bruls, H. Hintzen, G. de With, R. Metselaar, and J. van Miltenburg, J. Phys. Chem. Solids **62**, 783 (2001).

[25] Z. Lenčěš, K. Hirao, Y. Yamauchi, and S. Kanzaki, J. Am. Ceram. Soc. **86**, 1088 (2003).

[26] C. M. Fang, R. A. de Groot, R. J. Bruls, H. T. Hintzen, and G. de With, J. Phys.: Condens. Matter **11**, 4833 (1999).

[27] J. Y. Huang, L.-C. Tang, and M. H. Lee, J. Phys.: Condens. Matter **13**, 10417 (2001).

[28] Y. M. Basalaev and P. V. Demushin, J. Struct. Chem. **51**, 1191 (2010).

[29] Y. M. Basalaev, P. V. Demushin, E. V. Nikolaeva, and A. V. Silinin, Moscow Univ. Phys. Bull. (Engl. Transl.) **66**, 39 (2011).

[30] Y. M. Basalaev, P. V. Demushin, E. V. Nikolaeva, A. S. Poplavnoi, and A. V. Silinin, Russ. Phys. J. **54**, 1145 (2012).
[31] F. Arab, F. A. Sahraoui, K. Haddadi, A. Bouhemadou, and L. Louail, Phase Transitions **89**, 480 (2016).
[32] M. van Schilfgaarde, T. Kotani, and S. Faleev, Phys. Rev. Lett. **96**, 226402 (2006).
[33] X. Gonze, J. M. Beuken, R. Caracas, F. Detraux, M. Fuchs, G. M. Rignanese, M. Sindic, L.and Verstraete, G. Zerah, and F. Jollet, Comput. Mater. Sci. **25**, 478 (2002/11).
[34] J. P. Perdew and A. Zunger, Phys. Rev. B **23**, 5048 (1981).
[35] J. P. Perdew, K. Burke, and M. Ernzerhof, Phys. Rev. Lett. **77**, 3865 (1996).
[36] M. Fuchs and M. Scheffler, Comput. Phys. Commun. **119**, 67 (1999).
[37] M. Methfessel, M. van Schilfgaarde, and R. A. Casali, in *Electronic Structure and Physical Properties of Solids. The Use of the LMTO Method*, Lecture Notes in Physics, Vol. 535, edited by H. Dreyssé (Springer Verlag, Berlin, 2000), p. 114.
[38] T. Kotani and M. van Schilfgaarde, Phys. Rev. B **81**, 125117 (2010).
[39] M. van Schilfgaarde, T. Kotani, and S. V. Faleev, Phys. Rev. B **74**, 245125 (2006).
[40] T. Kotani, M. van Schilfgaarde, and S. V. Faleev, Phys. Rev. B **76**, 165106 (2007).
[41] Inorganic crystal structure database, Fachinformationszentrum, Eggenstein-Leopoldshafen 2, D-7514 Karlsruhe, Germany.
[42] P. Vinet, J. R. Smith, J. Ferrante, and J. H. Rose, Phys. Rev. B **35**, 1945 (1987).
[43] J. Heyd, G. E. Scuseria, and M. Ernzerhof, J. Chem. Phys. **118**, 8207 (2003).
[44] J. Heyd, G. E. Scuseria, and M. Ernzerhof, J. Chem. Phys. **124**, 219906 (2006).
[45] J. B. Quirk, M. Råsander, C. M. McGilvery, R. Palgrave, and M. A. Moram, Appl. Phys. Lett. **105**, 112108 (2014).
[46] M. Cardona and M. L. W. Thewalt, Rev. Mod. Phys. **77**, 1173 (2005).